Published in final edited form as:
J Control Release. 2008 August 7; 129(3): 228–236. doi:10.1016/j.jconrel.2008.04.024.

Super pH-sensitive Multifunctional Polymeric Micelle for Tumor pH_e Specific TAT Exposure and Multidrug Resistance

Eun Seong Lee[1,3], **Zhonggao Gao**[1], **Dongin Kim**[1], **Kyeongsoon Park**[2], **Ick Chan Kwon**[2], and **You Han Bae**[1,*]

1*Department of Pharmaceutics and Pharmaceutical Chemistry, University of Utah, Salt Lake City, 421 Wakara Way, Suite 315, UT 84108, USA*

2*Biomedical Research Center, Korea Institute of Science and Technology, 39-1 Hawolgok-dong, Seongbuk-gu, Seoul 136-791, Korea*

Abstract

As an alternative to cell specific cancer targeting strategies (which are often afflicted with the heterogeneity of cancer cells as with most biological systems), a novel polymeric micelle constitute of two block copolymers of poly(L-lactic acid)-*b*-poly(ethylene glycol)-*b*-poly(L-histidine)-TAT (transactivator of transcription) and poly(L-histidine)-*b*-poly(ethylene glycol) was developed. The micelle formed via the dialysis method was approximately 95 nm in diameter and contained 15 wt. % of doxorubicin (DOX) by weight. The micelle surface hides TAT during circulation, which has the strong capability to translocate the micelle into cells, and exposes TAT at a slightly acidic tumor extracellular pH to facilitate the internalization process. The micelle core was engineered for disintegration in early endosomal pH of tumor cells, quickly releasing DOX. The ionization process of the block copolymers and ionized polymers assisted in disrupting the endosomal membrane. This processes permitted high DOX concentrations in the cytosol and its target site of the nucleus, thus increasing DOX potency in various wild and multidrug resistant (MDR) cell lines (3.8–8.8 times lower IC_{50} than free DOX, depending on cell line). When tested with the xenografted tumors of human ovarian tumor drug-resistant A2780/AD, human breast tumor drug-sensitive MCF-7, human lung tumor A549 and human epidermoid tumor KB in a nude mice model, all tumors significantly regressed in size by three bolus injections at a dose of DOX 10 mg equivalent/kg body per injection of DOX-loaded micelle at three day interval, while minimum weight loss was observed. This approach may replace the need for cell-specific antibodies or targeting ligands, thereby providing a general strategy for solid tumor targeting.

Keywords

pop-up pH-sensitive polymeric micelle; Tumor pH; Triggering drug release; Multidrug resistance

*To whom correspondence should be addressed. 10, Tel: +(801)-585-1518, Fax: +(801)-585-3614, E-mail: you.bae@utah.edu.
[3]Current address: Division of Biotechnology, The Catholic University of Korea, 43-1 Yeokgok 2-dong, Bucheon-si, 420-743, Korea

1. Introduction

Tumor cells are often identified by over-expressed surface markers [1,2], including particular receptors that respond to various signals and nutrients present in their surrounding environment. Unique surface markers include tumor cell-specific antigens that can be specifically targeted by monoclonal antibodies or ligand/receptor pair interactions. The design of drug carriers targeting tumors have extensively exploited these paired cell-specific interactions (*e.g.*, antigen/antibody and ligand/receptor) to target macromolecular or nano-sized vehicles carrying cytotoxic drugs for internalization into tumor cells via intracellular delivery mediated by various active endocytotic pathways [3]. The repertoire of interactions for drug targeting is rather limited because solid tumors display rather heterogeneous cell populations as well as differential antigen or receptor expression on cell surfaces [4–7]. For example, HER2 antigen (human epidermal growth factor receptor 2 protein) currently used for breast tumor targeting is positive in only 20–30% of human breast tumor [4]. Moreover, normal cells often express the same antigens or receptors as do the tumor cells [5,6]. As an example, the tumor necrosis factor-related apoptosis-inducing ligand (TRAIL) has been exploited for therapy since it induces apoptosis in tumor cells [5]. However, recent findings that healthy human hepatocytes, brain tissue, and certain epithelial cells are also susceptible to TRAIL have raised serious concerns of its potential toxicity if administered systemically [5]. Folate has also been explored as a targeting moiety since expression of folate receptor is positive in approximately 89% of human ovarian tumors and in approximately 20–50% of solid tumors originated from kidney, lung tumor, breast, bladder, and pancreas. However, this marker is not ubiquitous since the folate receptor is essentially absent in ovarian tumor [6]. Moreover, ‘positive’ bioassays for folate receptor are not sensitive enough to discriminate between expression levels that are sufficiently high to produce active cell entry upon binding. Together, these factors clarify why various drug delivery systems targeting tumor cell-specific antigens or receptors produce mixed outcomes and limited efficacy in clinical settings [7].

The TAT peptide is one of non-specific cell penetrating peptides [8], derived from human immunodeficiency viruses types 1 and 2 (HIV-1 and HIV-2), that has been reported to be a potent transcriptional activator of viral gene expression [9]. TAT peptide serves to quickly translocate various attached molecules into mammalian cells both *in vitro* and *in vivo* [9,10]. Although the precise entry pathways are still controversial, small molecules attached to TAT peptide are likely to be internalized into cells by passive electrostatic interactions [11] whereas TAT-polymer conjugates and TAT-conjugated nano-sized drug carriers are thought to be taken up by energy-dependent endocytosis (or macropinocytosis) after electrostatic interactions [12]. Recently, researchers have challenged the use of TAT for *in vivo* applications, however their results do not support the *in vivo* efficacy of TAT based delivery systems [11,12]. One of the main obstacles that still remains unresolved is the lack of selectivity of TAT [11,12].

We previously reported a pH-sensitive pop-up polymeric micelle system which presents a targeting moiety such as biotin on its surface in response to small change in pH [13]. Above pH 7.2 biotin was anchored on the inside of the polymeric micelle via a pH-sensitive molecular chain actuator - a short poly(L-histidine) (polyHis), thus being shielded by the poly(ethylene glycol) (PEG) shell of the micelle. When the pH becomes slightly more acidic ($6.5<pH<7.2$), the actuator becomes charged and exposes the biotin to the outside of PEG shell, and where it interacts with avidin and tumor cells. This event facilitated biotin receptor-mediated endocytosis in cells. When the pH is further lowered ($pH<6.5$), the micelles become physically destabilized, which results in enhanced drug release, disruption of the cell’s endosomal membrane [13–16], and increase intracellular drug concentration [13,14].

These previous results prompted us to examine a more universal delivery and entry strategy for various solid tumors by introducing a non-specific cell penetrating peptide (TAT peptide) to the super pH-sensitive pop-up polymeric micelle system.

Acidic pH is known to be a prominent microenvironment in solid tumors. Typical extracellular pH (pH_e) ranges from 7.0 to 6.5 in both tumor xenograft animal models [13,14,17] and in clinical tumors [17]. This acidic pH is thought to be a tumor phenotype caused by anaerobic respiration and subsequent glycolysis [17,18]. In particular, tumor pH_e (but not normal tissues) may be lowered by 0.2–0.4 pH units by glucose given orally or intravenously [19]. Weakly acidic pH, in the range of 7.0-6.8, is the natural pH range used for targeting purposes to most solid tumors in both animal models and humans, and this pH range can be used in clinical patients, optionally with a glucose challenge if necessary to induce lower pH.

2. Materials and methods

2.1 Materials

Cystamine, triscarboxyethylphosphine (TCEP), N-(2-aminoethyl) maleimide (AEM), succinic anhydride, triethylamine (TEA), 4-dimethylaminopyridine (DMAP), *N*,*N*′′-dicyclohexylcarbodiimide (DCC), *N*-hydroxysuccinimide (NHS), folate, pyridine, sodium, liquid ammonia, dimethylsulfoxide (DMSO), dimethylformamide (DMF), dichloromethane (DCM), diethyl ether, tetrazolium salt MTT, FITC (fluorescein isocyanate), ammonium chloride, L-glutamine, and DOX·HCl were purchased from Sigma-Aldrich (St. Louis, MO, USA). Penicillin–streptomycin, fetal bovine serum (FBS), 0.25% (w/v) trypsin–0.03% (w/v) EDTA solution, and RPMI1640 medium were purchased from Gibco (Uxbridge, UK). Cy5.5 Bis NHS ester was provided by GE healthcare (Piscataway, NJ, USA). LysoTracker Red DND-99 and *N*-(fluorescein-5-thiocarbamoyl)-1,2-dihexadecanoyl-*sn*-glycero-3-phosphoethanolamine, triethyl ammonium salt (fluorescein DHPE) were purchased from Invitrogen (Carlsbad, CA, USA). TAT peptide (FITC-Gly-Cys-$(Gly)_3$-Tyr-Gly-Arg-$(Lys)_2$-$(Arg)_2$-Gln-$(Arg)_3$) was provided from the protein synthesis core facility at the University of Utah.

2.2. Polymer synthesis (Supplementary Information, Scheme S-1)

2.2.1. Synthesis of poly(benzyl-His)(2kDa)—Poly(^{im}benzyl-L-histidine)-maleimide (Mal) (2kDa) (poly(benzyl-His)(2kDa)-Mal) was synthesized by ring-opening polymerization of protected His N-carboxyanhydride (NCA) using AEM as a initiator. His NCA (30 mmol) prepared as described in detail in our previous reports [13,20,21] was dissolved in DMF (20 ml) in the presence of AEM (1 mmol) and reacted for 3 days at room temperature. After reaction, diethyl ether was added to the solution to precipitate the product. The molecular weight of poly(benzyl-His)-Mal was targeted to 2kDa (Supplementary Information, Table S-1), measured as described before [13,20,21].

2.2.2. Synthesis of Mal-polyHis(2kDa)-Mal—The terminal amine group of poly(benzyl-His)(2kDa)-Mal (20 mmol) was modified with succinic anhydride (24 mmol), DMAP (24 mmol), and TEA (24 mmol) in DMF (30 ml)/pyridine (10ml) at room temperature for 1 day. After the reaction, the carboxylated poly(benzyl-His)(2kDa)-Mal (yield: 96±3 wt.%) was obtained after recrystallization from excess diethyl ether. The conversion of the terminal amino group of poly(benzyl-His)(2kDa)-Mal into a carboxyl group was confirmed by the transfer of the ^{1}H NMR peak at δ 3.97 (-C**H**-NH_2 at the terminal site of poly(benzyl-His)(2kDa)) to δ 4.92 (-C**H**-NH-CO- at the conjugation site of poly(benzyl-His)(2kDa) and succinic anhydride). In order to substitute a carboxyl group in poly(benzyl-His)(2kDa)-Mal with AEM, the carboxylated poly(benzyl-His)(2kDa)-Mal (20 mmol) was pre-activated using NHS (24 mmol) and DCC (24 mmol) in DMF (30 ml). After carrying out the reaction for 1 day at room

temperature, dicyclohexylurea (DCU) was removed by filtration and then AEM (40 mmol) suspended in TEA (40 mmol) was added to the filtrate for coupling reaction between poly (benzyl-His)(2kDa)-Mal and AEM (reaction time: one day). The solution was then dialyzed to remove unconjugated AEM. Mal-poly(benzyl-His)(2kDa)-Mal (yield: 94±5 wt.%) was obtained after freeze-drying. ^{1}H-NMR showed peak transfer of δ 4.12 (-C**H**$_2$-COOH, terminal group of the carboxylated poly(benzyl-His)(2kDa)) to δ 2.04 (-C**H**$_2$-CO-NH-Mal, conjugation site). The percentual conversion of poly(benzyl-His)-Mal to Mal-poly(benzyl-His)-Mal was 95±3 wt.%, as calculated by the comparison of ^{1}H NMR peak of δ 4.92 (-CO-C**H**-NH-, repeating units of polyHis) and δ 6.95 (-C**H**=C**H**-at Mal group). Subsequently, Mal-poly (benzyl-His)(2kDa)-Mal (2 g) was treated with finely cut metallic sodium (0.4 g) under anhydrous liquid ammonia (40 ml) to remove benzyl groups in poly(benzyl-His)(2kDa) (reaction time: 30 min) [13,20,21]. Residual (non-reacted) sodium was discharged with ammonium chloride (0.1 g). After evaporating all liquid ammonia, 1 N HCl (15 ml) was added to dissolve the residue. This solution was filtered to remove insoluble materials and extracted three times with diethyl ether (40 ml) to remove byproduct (reductive benzyl group). Mal-polyHis(2kDa)-Mal (yield: 87±6 wt.%) was collected after freeze-drying for 2 days. The removal of benzyl group was confirmed by ^{1}H-NMR peaks: no peak of δ 7.2 (benzyl group). In addition, to determine molecular weight of polymer, MALDI TOF mass spectra (from a Micromass TOFSPEC mass spectrometer in the reflection mode) were analyzed. A PEG mixture, consisting of PEG 650, 1500 and 4100 were used for calibration. As a result, M_n and polydispersity index (PDI) of Mal-polyHis-Mal were 1,983 and 1.23, respectively.

2.2.3. Synthesis of PLA(3kDa)-b-PEG(2kDa)-SH—Poly(L-lactic acid) (3kDa)-*b*-PEG (2kDa)-COOH (PLA(3kDa)-*b*-PEG(2kDa)-COOH) was prepared by a conventional method [13,20,21]. PLA(3kDa)-*b*-PEG(2kDa)-COOH (20 mmol) pre-activated with NHS (24 mmol) and DCC (24 mmol) was reacted with cystamine (40 mmol) in DMSO (15 ml), in the presence of TEA (40 mmol). After 1 day, TCEP (80 mmol) dissolved in deionized water (30 ml) was mixed with the solution for the reduction of PLA(3kDa)-*b*-PEG(2kDa)-cystamine-PEG (2kDa)-*b*-PLA(3kDa) or PLA(3kDa)-*b*-PEG(2kDa)-cystamine (reaction time: 4 hours). The solution was then dialyzed to remove unconjugated cystamine and TCEP. PLA(3kDa)-*b*-PEG (2kDa)-SH (yield: 70±8 wt.%) was lyophilized. PLA(3kDa)-*b*-PEG(2kDa)-SH was examined using ^{1}H-NMR. ^{1}H-NMR showed peak transfer of δ 4.23 (-C**H**$_2$-COOH, terminal group of PLA(3kDa)-*b*-PEG(2kDa)-COOH) to δ 2.83 (-C**H**$_2$-CO-NH-, conjugation site of PLA(3kDa)-*b*-PEG(2kDa)-SH). The percentual conversion of PLA(3kDa)-*b*-PEG(2kDa)-COOH to PLA (3kDa)-*b*-PEG(2kDa)-SH was 82±5 wt.%, as calculated by the comparison of two ^{1}H NMR peaks (δ 4.23 and δ 2.83).

2.2.4. Synthesis of PLA(3kDa)-b-PEG(2kDa)-b-polyHis(2kDa)-Mal—The coupling of Mal-polyHis(2kDa)-Mal (75 mmol) and PLA(3kDa)-*b*-PEG(2kDa)-SH (25 mmol) was carried out in DMSO/water (20 ml/2 ml) for overnight. The resulting solution was dialyzed against excess DMSO using a dialysis membrane tube (Spectra/Pore; MWCO 5kDa) to remove unconjugated polymers. The solution in a dialysis membrane tube was then dialyzed against excess deionized water with 6 M TCEP for the reduction of PLA(3kDa)-*b*-PEG(2kDa)-S-S-PEG(2kDa)-*b*-PLA(3kDa) for 8 hours. The resulting solution in a dialysis membrane tube was then dialyzed against excess DMF using a dialysis membrane tube (Spectra/Pore; MWCO 5kDa) to remove PLA(3kDa)-*b*-PEG(2kDa)-SH for 1 day. The 8-fold excess diethyl ether was added to the solution to precipitate the product. After freeze-drying, PLA(3kDa)-*b*-PEG (2kDa)-*b*-polyHis(2kDa)-Mal (yield: 80± 4 wt.%) was obtained. The DMSO-mediated oxidation of SH group to disulfide (-S-S-) may be occurred as a side reaction during the conjugation [22]. However, the addition of 6-fold excess Mal for SH group seemed to facilitate the chemical reaction between Mal- and SH- group. The coupling of Mal-polyHis(2kDa)-Mal and PLA(3kDa)-*b*-PEG(2kDa)-SH was confirmed by the presence of ^{1}H NMR peak at δ 3.24

(-CH-C**H**$_2$-, maleimide reacted with –SH group), considering that peak of -C**H**=C**H**- in maleimide group was shown at δ 6.95. The M_n and PDI of PLA(3kDa)-b-PEG(2kDa)-b-polyHis(2kDa)-Mal were analyzed to 7,232 and 1.45, as measured by MALDI TOF mass spectra. The presence of byproduct, PLA(3kDa)-*b*-PEG(2kDa)-*b*-polyHis(2kDa)-*b*-PEG (2kDa)-*b*-PLA(3kDa) were less than 1%, confirmed by the above two ^{1}H NMR peaks.

2.2.5. Synthesis of PolyHis(5kDa)-b-PEG(3.4kDa)—PolyHis(5kDa) was synthesized by ring-opening polymerization of protected His NCA using isopropylamine as a initiator [13,20,21]. The polymer block was then coupled with PEG(3.4kDa) via an amide bond as describe before [13,20,21]. Next, the protecting (benzyl) group of polyHis was deprotected using sodium and liquid ammonia as described before [21].

2.2.6. Synthesis of PLA(3kDa)-b-PEG(3.4kDa) and PLA(3kDa)-b-PEG(3.4kDa)-folate—PLA(3kDa)-*b*-PEG(3.4kDa) and PLA(3kDa)-*b*-PEG(3.4kDa)-folate was prepared using standard methods [13,20,21].

2.2.7. Synthesis of PLA(3kDa)-b-PEG(3.4kDa)-Mal—PLA(3kDa)-*b*-PEG(2kDa)-COOH (20 mmol) pre-activated with NHS (24 mmol) and DCC (24 mmol), was reacted with AEM (40 mmol) in DCM (15 ml), in the presence of TEA (40 mmol). After 1 day, the solution was filtered to remove DCU and recrystallized from excess diethyl ether. PLA(3kDa)-*b*-PEG (2kDa)-Mal (yield: 90±8 wt.%) was obtained after vacuum-drying. ^{1}H-NMR showed peak transfer of δ 4.23 (-C**H**$_2$-COOH, terminal group of PLA(3kDa)-*b*-PEG(3.4kDa)-COOH) to δ 2.05 (-C**H**$_2$-CO-NH-Mal, terminal group of PLA(3kDa)-*b*-PEG(3.4kDa)-Mal) and included maleimide peaks at δ 6.95.

2.3. Polymeric micelle preparation

2.3.1. TAT pop-up pH-sensitive micelles (denoted as PHSM$^{pop\text{-}upTAT}$ hereafter)—PLA(3kDa)-*b*-PEG(2kDa)-*b*-polyHis(2kDa)-Mal (40 mol%), polyHis(5kDa)-*b*-PEG (3.4kDa) (60 mol%) and DOX dissolved in DMSO (75 vol%) were coupled with TAT (FITC) (40 mol%) dissolved in $Na_2B_4O_7$ buffer solution (pH 9.0, 20 mM) (25 vol%) for 6 hours at room temperature. PLA(3kDa)-*b*-PEG(2kDa)-*b*-polyHis(2kDa)-TAT in solution was formed from the chemical reaction [23] between maleimide group of PLA(3kDa)-*b*-PEG(2kDa)-*b*-polyHis(2kDa)-Mal and TAT's cysteine. The mixed solution was transferred to a pre-swollen dialysis membrane tube (Spectra/Por; MWCO 15kDa) and dialyzed against $Na_2B_4O_7$ buffer solution (pH 7.4, 20 mM) for constituting micelles and removing unconjugated TAT. The outer phase was replaced three times with fresh $Na_2B_4O_7$ buffer solution for 24 hours [24,25]. The micellar solution was lyophilized. The critical micelle concentration was 3 μg/ml, calculated from a published pyrene fluorescent study [13,20,21].

2.3.2. pH-sensitive micelles lacking TAT peptide (denoted as PHSM)—PLA (3kDa)-*b*-PEG(2kDa)-*b*-polyHis(2kDa) (40 mol%), polyHis(5kDa)-*b*-PEG(3.4kDa) (60 mol %) and DOX dissolved in DMSO was dialyzed to construct PHSM as described above.

2.3.3. pH-sensitive micelles that expose TAT peptide at all pH ranges (denoted as PHSM^{TAT})—PLA(3kDa)-*b*-PEG(3.4kDa)-Mal (40 mol%), polyHis(5kDa)-*b*-PEG (3.4kDa) (60 mol%) and DOX dissolved in DMSO were reacted with TAT (40 mol%) and were dialyzed to construct PHSM^{TAT}.

2.3.4. pH-sensitive micelles that expose folate at all pH ranges (denoted as PHSM^{folate})—PLA(3kDa)-*b*-PEG(3.4kDa)-folate (40 mol%), polyHis(5kDa)-*b*-PEG (3.4kDa) (60 mol%) and DOX dissolved in DMSO were dialyzed to construct PHSM^{folate} [26,27].

2.3.5. pH-insensitive micelles that expose TAT peptide at all pH ranges (denoted as PHIM^{TAT})—PLA(3kDa)-*b*-PEG(3.4kDa)-Mal (40 mol%), PLA(3kDa)-*b*-PEG(3.4kDa) (60 mol%) and DOX dissolved in DMSO were reacted with TAT (40 mol%) and were dialyzed to construct PHIM^{TAT}.

2.3.6. pH-insensitive micelles (denoted as PHIM)—PLA(3kDa)-*b*-PEG(3.4kDa) and DOX dissolved in DMSO were dialyzed to construct PHIM.

2.4. Coupling TAT peptide to micelles

The yield of TAT conjugation was measured from fluorescence (excitation: 485 nm; emission=535 nm) intensity of micelles dissolved in DMSO, based upon a standard curve of fluorescence intensity of free TAT (FITC) with concentration. Results showed 90–95 wt.-% of TAT feed was conjugated to polymeric micelles.

2.5. DOX loading and DOX release test

10 When a total 5 mg of polymer with DOX (1 mg) was dialyzed to produce micelles, 0.80–0.90 mg of DOX was encapsulated into the micelles [26,27]. For DOX release test, the micelles in a dialysis membrane tube (Spectra/Por MWCO 5kDa) including PBS pH 7.4 solution (0.5 ml, ionic strength: 0.15) were immersed in a vial containing fresh PBS (50 ml) with different pHs (pH 8.0-6.0) for 24 hours including mechanical shaking (100 *rev.* /min) at 37 °C. The measurement of DOX concentration in micelles was performed with a UV/visible spectrophotometer as described previously [24,25].

2.6. Cell culture

Human breast tumor MCF-7 cells (from ATCC), drug-resistant NCI/ADR-RES cells (from NCI), human ovarian tumor A2780 cells (from ATCC), drug-resistant A2780/AD cells (kindly supplied by Prof. Kopecek, Univ. Utah), human promyelocytic leukemia HL-60 cells, drug-resistant HL-60/MX2 (from ATCC), human lung tumor drug-resistant NCI-H69/AR cells (from ATCC), human lung tumor A549 cells (from ATCC) and human epidermoid tumor KB cells (from ATCC) were maintained in RPMI-1640/PBS medium with 0.5M PBS, 2 mM L-glutamine, 5% penicillin–streptomycin, 10% fetal bovine serum in a humidified incubator at 37 °C and 5% CO_2 atmosphere. Before testing, cells (1×10^5 cells/ml) growing as a monolayer were harvested by trypsinization using a 0.25% (w/v) trypsin–0.03% (w/v) EDTA solution. Cells suspended in RPMI-1640 medium (200 μl) were seeded into a 96-well plate and cultured for 24 hours prior to *in vitro* cell testing.

2.7. Cellular uptake of polymeric micelles

TAT (FITC) was linked to PHSM$^{pop\text{-}upTAT}$ for fluorescent cellular uptake studies. MCF-7 cells (1×10^6 cells/ml) in 96-well plates were treated with PHSM$^{pop\text{-}upTAT}$ (FITC) suspensions for a specified times. The pH of RPMI-1640 culture medium was adjusted with PBS 0.5 M, HCl and NaOH [26,27]. The cells were then washed with PBS (pH 7.4) and lysed using 125 μl CellLyticiM Cell Lysis Reagent (Gibco). Fluorescein uptake (% FITC uptake) was measured by assaying the cell lysate using static fluorescence measurements (excitation and emission wavelengths of 488 and 520 nm, respectively), based upon a standard curve of fluorescence intensity of free TAT (FITC) with concentration. All fluorescence intensities were normalized to total cell protein (*g*) calculated from a standard BCA protein assay kit (Gibco) [24,25]. Furthermore, PHSM without TAT was investigated as a control group. The FITC was directly conjugated to PHSM for the fluorescence study as described in detail in our previous report [13]. Fluorescein uptake was measured by assaying the cell lysate using static fluorescence measurements, based upon a standard curve of fluorescence intensity of free FITC with

concentration. All fluorescence intensities were also normalized to total cell protein (*g*) calculated from a standard BCA protein assay kit.

2.8. Cell cytotoxicity

Free DOX or equivalent DOX-loaded micelles ($PHSM^{pop\text{-}upTAT}$, PHSM, $PHSM^{TAT}$, $PHIM^{TAT}$ and PHIM) dispersed in RPMI-1640/PBS medium with different pH values (pH 7.4-6.4) were added to cells plated in 96-well plates for cell cytotoxicity testing. The pH of the culture medium was adjusted to each corresponding pH during the assay as described before [24,25]. Cell cytotoxicity as measured using the MTT assay [24,25]. Cell viability (%) was calculated by dividing number of live cells (after being treated with DOX or DOX-loaded micelles) with number of live cells (existing in drug-free culture medium) at each pH after 48-hour incubation.

2.9. Animal care

In vivo studies were performed in 4–6 weeks old female nude mice (BALB/c nu/nu mice, Charles River Lab, Wilmington, USA). Nude mice were maintained under the guidelines of an approved protocol from the University of Utah Institutional Animal Care and Use Committee.

2.10. Dorsal skin window chamber model

To investigate *in situ* the delivery of polymeric micelles to solid tumors, the noninvasive visualization method of 'dorsal skin fold window chamber model' was employed [28]. To establish the dorsal skin fold window chamber model [29], a flap of skin measuring 1 cm in diameter was dissected away from opposing surfaces of the dorsal skin flap of an anesthetized mouse, leaving a facial plane with associated vasculature. The flaps were held vertically away from the body with an aluminum or titanium saddle, which was sutured to both sides of the flap. MCF-7 tumor cells or small tumor pieces (~ 1 mm^3) extracted from xenograft mice bearing MCF-7 were implanted into the window chamber. Glass windows were then attached to the center of the saddle to cover the surgical site. After surgery, the skin surfaces adjacent to the window assembly were covered with neomycin sulfate ointment to prevent infection [28,29]. In addition, fluorescein DHPE was incorporated into the polymeric micellar core for precise fluorescent imaging micelles in skin dorsal window. Polymers and fluorescein DHPE were dissolved in DMSO and were dialyzed to construct FITC labeling micelles as described above.

For serial observation of the window, nude mice intravenously administered with FITC-labeled micelles ($PHSM^{pop\text{-}upTAT}$ or $PHSM^{TAT}$) (60 mg micelle per kg body) were anesthetized with a mixture of 90 mg/kg ketamine (Abbott, IL, USA) and 10mg/kg xylazine (Bayer, KS, USA). Nude mice were placed on a glass stage with an adjustable restrainer and kept warm using a temperature-controlled heating blanket (homeothermic system, Harvard Apparatus) at 37°C on the microscope stage. Nude mice were positioned so that the mammary window was aligned with the hole of a restraining bar. Observation was made using intravital fluorescence microscopy (Olympus BX51WI Microscope, Leeds Precision Instruments, Inc. MN) over time.

2.11. NIR fluorescence real-time tumor imaging

Cy5.5® (fluorescent dye for precise *in vivo* imaging) bis-NHS ester (2 mol) was reacted with primary amines of poly(benzyl-His)(5kDa) (1 mol) in water/DMSO (1ml/5 ml) mixture solution for 8 hours. After the reaction, unconjugated Cy5.5® bis-NHS ester was removed by dialysis. Cy5.5® labeled poly(benyzl-His) was lyophilized from freeze-drying.

Preparation of Cy5.5® labeled $PHSM^{pop\text{-}upTAT}$ was performed with Cy5.5® labeled poly (benzyl-His) (10 mol%), PLA(3kDa)-*b*-PEG(2kDa)-*b*-polyHis(2kDa)-TAT (40 mol%),

polyHis(5kDa)-*b*-PEG(3.4kDa) (50 mol%) and DOX. Preparation of Cy5.5® labeled $PHSM^{TAT}$ was performed with Cy5.5® labeled poly(benzyl-His) (10 mol%), PLA(3kDa)-*b*-PEG(3.4kDa)-TAT (40 mol%), polyHis(5kDa)-*b*-PEG(3.4kDa) (50 mol%) and DOX. 0.9 M NaCl was added to micelle solution for *in vivo* injection.

For *in vivo* animal experiments, KB cell tumors were introduced into female nude mice by subcutaneous injection of 1×10^6 cells suspended in cell culture media (RPMI-1640, 10% fetal bovine serum). When the tumor volume in two sites reached 50–70 mm^3, Cy5.5® labeled micelles (60 mg micelle per kg body) were intravenously injected into KB tumor-bearing nude mice through a tail vein.

After *i.v.* administration of Cy5.5® labeled micellar solutions, the time-dependent tissue distribution in tumor-bearing nude mice was imaged by positioning nude mice on an animal plate heated to 37°C using the Explore Optix System (ART Advanced Research Technologies Inc., Montreal, Canada). Nude mice were automatically moved to the imaging chamber for scanning. Laser power and count time settings were optimized at 25 mW and 0.3 sec per point. Excitation and emission spots were raster-scanned in 1 mm steps over the selected region of interest to generate emission wavelength scans. A 670 nm pulsed laser diode was used to excite Cy5.5® molecules. NIR fluorescence emission at 700 nm was collected and detected with a fast photo multiplier tube (Hamamatsu, Japan) and a time-correlated single photon counting system (Becker and HicklGmbH, Berlin, Germany) [30].

2.12. Tumor inhibition assays

To establish xenograft mice bearing various tumors, 1×10^6 cells (A2780/AD, MCF-7, or A549 cells) suspended in cell culture media (RPMI-1640, 10% fetal bovine serum) were subcutaneous injected into the left inguinal mammary line. After 2 weeks, tumors were grown to 50~100 mm^3. Free DOX or DOX-loaded micelles ($PHSM^{pop\text{-}upTAT}$, PHSM, $PHSM^{TAT}$, and $PHSM^{folate}$) were intravenously injected into tumor-bearing nude mice through a tail vein at a 3-day interval (e.g., 0, 3, and 6 days post the first injection). The injection volume (approximately 0.2 ml/10g body weight) of micelle solution was adjusted to yield 10 mg DOX per kg of body weight. Tumor volume and mouse weight were monitored with elapsed time. A mean standard error was calculated for each experimental point. Tumor volume was calculated using the formula: tumor volume=length×$(\text{width})^2/2$. The dimension of the tumor was measured using an electronic digital caliper [25].

2.13. Statistical analysis

All results were analyzed by student t-test or ANOVA test with $p < 0.05$ significance. MINITAB® *release 14* statistical software was used.

3. Results and discussion

3.1. pH-sensitivity

Various combinations of the synthetic polymers comPprising the micelle carrier for TAT surface repositioning triggered by pH_e were engineered and optimized (Fig. 1A) [13]. The $PHSM^{pop\text{-}upTAT}$ (~ 95 nm size in diameter, measured by dynamic light scattering) is formed by self-assembly of a mixture of two block copolymers (poly(L-lactic acid)(PLA)(3kDa)-*b*-PEG(2kDa)-*b*-polyHis(2kDa)-TAT and polyHis(5kDa)-*b*-PEG(3.4kDa)) by dialysis methods. Herein, the numerical values in parentheses indicate the molecular weight of each block (for example, 3kDa means 3,000 Daltons). This micelle comprises a hydrophobic core (PLA(3kDa) and polyHis(5kDa) blocks), a hydrophilic corona or shell (PEG(2kDa) and PEG(3.4kDa) blocks) and a TAT peptide repositioning actuator (polyHis(2kDa) block) (Fig. 1A). The ionization state of the polyHis(2kDa) block determines the positioning of the TAT peptide in

the micelle. At pH 7.4 TAT is shielded within the hydrophilic PEG corona shell by interfacial hydrophobic interactions between non-ionized polyHis(2kDa) and PLA micelle core. However, the micelles expose TAT on their surface when polyHis(2kDa) becomes ionized at pH_e, prior to ionization of the longer polyHis(5kDa) block blended with PLA in the micellar core (Fig. 1A). TAT exposure by the $PHSM^{pop\text{-}upTAT}$ was examined by observing cellular uptake of the micelles as pH of the medium was reduced (Fig. 1B). At pH 7.4, micelle uptake by human breast tumor drug-sensitive MCF-7 cells was minimal. At pH 7.0, cell uptake increased 30-fold compared to that at pH 7.4, attributed to the partial exposure of TAT on the micellar surface. At pH 6.8, there was a 70-fold increase. These results are comparable with the PHSM. It was found that the effect of pH in a culture medium on cellular uptake of PHSM is negligible: 2.1±0.6 ((%) FITC (fluorescein isocyanate) uptake per (g) protein) at pH 7.4 and 2.9±0.5 ((%) FITC uptake per (g) protein) at pH 6.8 after 48 hours (data not shown). In addition, it was also observed that the effect of pH in culture medium on cellular uptake of the $PHSM^{TAT}$ (~ 105 nm size in diameter) is negligible: 73±5 ((%) FITC uptake per (g) protein) at pH 7.4 and 72±4 ((%) FITC uptake per (g) protein) at pH 6.8 (data not shown). Furthermore, the $PHSM^{pop\text{-}upTAT}$ showed triggered DOX release at acidic pH (Fig. 1C). At pH 7.4-7.0 the $PHSM^{pop\text{-}upTAT}$ showed limited DOX release. However, at pH 6.6 the $PHSM^{pop\text{-}upTAT}$ released 60 wt.% of the initial DOX amount and at pH 6.4 (*e.g.*, endosomal pH) the $PHSM^{pop\text{-}upTAT}$ released approximately 78 wt.% of the initial DOX amount. These pH-sensitive DOX release properties of $PHSM^{pop\text{-}upTAT}$ are due to the physical destabilization of the hydrophobic core (resulting from ionization of polyHis) as the pH decreases [20–25]. In addition, DOX release behaviors of the PHSM or $PHSM^{TAT}$ with pH were similar to that of the $PHSM^{pop\text{-}upTAT}$ (data not shown).

Further evidence of the efficacy is shown in Fig. 1D which displays the pH-dependent cytotoxic effects produced by the model anticancer drug, DOX incorporated within the $PHSM^{pop\text{-}upTAT}$ (DOX: ~15 wt.% in micelle) on MCF-7 cells in culture. At the weakly acidic pH of 7.0 and 6.8, $PHSM^{pop\text{-}upTAT}$ showed 2 and 8 times higher cytotoxicity, respectively, than that seen at the physiological pH of 7.4. This is presumably due to enhanced cellular uptake rates of $PHSM^{pop\text{-}upTAT}$ when the TAT peptide is exposed as shown in Fig. 1B. At pH 6.4, the endosomal pH, the $PHSM^{pop\text{-}upTAT}$ is further destabilized because of the ionization of polyHis (5kDa) in the micellar core [24,25], this leads to release of more drug into the medium, and results in less active internalization of drug and less cytotoxicity, but still greater cytotoxicity than free DOX. While the PHSM (~87 nm size in diameter) showed 70% cell viability at pH 6.8, cell viability was reduced to 30% at pH 6.4 due to accelerated drug release by micelle destabilization at the outside of cells. Further the $PHSM^{TAT}$ showed the highest cytotoxicity, however the pH sensitivity was lost. The $PHIM^{TAT}$ (~ 101 nm size in diameter) and the PHIM (~ 80 nm size in diameter) were also used as controls and exhibited marginal MCF-7 cell killing efficacies. In addition, the effect of the DOX dose on pH-sensitivity of micelles was not significant (Supplementary Information, Fig. S-1). All blank micelles without DOX showed no cytotoxicity for MCF-7 cells at all pH ranges (cell viability ~100%) (data not shown).

From these observations, we conclude that (*i*) when the TAT peptide is exposed due to lowering of the pH into a narrow pH range (pH 7.0-6.8), extensive cellular uptake of the $PHSM^{pop\text{-}upTAT}$ by tumor cells is evident and (*ii*) when the pH is lowered further into the early endosomal pH range (pH<6.5), the $PHSM^{pop\text{-}upTAT}$ is destabilized further leading to the enhanced release of DOX. This then further exerts an endosomolytic effect produced by disassembled ionized polyHis segments [13,24,25]. These combined effects lead to more effective treatment for both drug-sensitive tumor cells. Shielding TAT peptide in a hydrophilic shell (Fig. 1A) in the blood (pH 7.4) is expected to minimize unwanted uptake of $PHSM^{pop\text{-}upTAT}$ by normal organs.

3.2. Overcoming MDR

A variety of multidrug resistance (MDR) mechanisms occurring at the unicellular level are known, including altered expression of topisomerase II (Topo II) and over-expression of P-glycoprotein (Pgp) (ATP-dependent efflux pumps), multidrug resistance protein (MRP), lung resistance protein (LRP), and antiapototic (or survival) bcl-2 protein [26,27,31]. In clinical settings, various factors in the microenvironment of tumors such as epidermal growth factor, fibroblast growth factor, insulin-like growth factor, and extracellular matrix components are strongly linked to the survival mechanisms of both tumor cells and normal healthy cells [26, 27]. These environmental factors are believed to be relevant to oncogenic survival pathways (*i.e.*, bcl-2 gene expression). Reversing MDR by bypassing a particular mechanism, for instance Pgp modulators, has been extensively studied, but a practical solution to defeat all of the many MDR mechanisms remains elusive [32]. One possible more general solution involves using a sufficiently high cytosolic dose of a conventional anticancer drug such that the common resistance mechanisms are overwhelmed. To further test this hypothesis, the $PHSM^{pop\text{-}upTAT}$ was tested in treating a series of different MDR tumor cell lines.

Fig. 2 shows the cytotoxic activity of the $PHSM^{pop\text{-}upTAT}$ against human breast tumor drug-resistant NCI/ADR-RES cells (from NCI) that over-expresses the drug efflux pump, Pgp, on the plasma membrane [26,31]. Free DOX is inactive against this cell line due to the enhanced Pgp activity. The efficacy of the $PHSM^{pop\text{-}upTAT}$ for NCI/ADR-RES cells was pH-dependent. $PHSM^{pop\text{-}upTAT}$ at pH 7.0 and 6.8 showed 2.2 and 8 times higher cytotoxicity than at pH 7.4, respectively. The results are similar to those obtained with MCF-7 cells (Fig. 1D) because TAT peptide-mediated endocytosis evades Pgp function [25].DOX prematurely released from $PHSM^{pop\text{-}upTAT}$ at pH 6.4 is less effective due to Pgp action in NCI/ADR-RES cells. On the other hand, the $PHIM^{TAT}$ and the PHIM did not show any significant cytotoxicity against these drug-resistant cells. In addition, the effect of the DOX dose on pH-sensitivity of micelles was not significant (Supplementary Information, Fig. S-2). All blank micelles without DOX showed no cytotoxicity for NCI/ADR-RES cells at all pH ranges (cell viability ~100%) (data not shown).

Similarly, as shown in Fig. 3, the $PHSM^{pop\text{-}upTAT}$ was able to overcome various MDR mechanisms, including over-expression of Pgp, altered Topo II expression, positive bcl-2 expression, MRP and LRP to demonstrate good killing efficacies. In contrast, the killing efficacies of drug-loaded control micelles were found to be worse than free DOX. In addition, Table 1 shows IC50 values of $PHSM^{pop\text{-}upTAT}$ and free DOX used in this study, indicating high cytotoxicity of $PHSM^{pop\text{-}upTAT}$ for MDR cells.

3.3. In vivo tumor inhibition

In order to evaluate the *in vivo* efficacy of the $PHSM^{pop\text{-}upTAT}$ for MDR solid tumors, human ovarian tumor drug-resistant A2780/AD cell xenografts in female nude mice were tested. Fig. 4A shows the *in vivo* results for the anti-tumor activity of DOX carried by the $PHSM^{pop\text{-}upTAT}$ injected intravenously on days 0, 3 and 6 in nude mice bearing the A2780/AD solid tumors. The drug dose in the micelle formulations was equivalent to 10 mg DOX/kg body, and the diluted polymer concentration (60 mg/kg body) in blood (blood volume ~7% of body weight) immediately after injection was approximately 280 times higher than the critical micelle concentration of 3 μg/ml. This treatment led to significant regression of the A2780/AD tumors. The tumor volume on week 3 was approximately 18 times smaller than that observed with the free DOX treatment ($P < 0.01$) and 7 and 6 times smaller than those treated with the control micelles (PHSM or $PHSM^{TAT}$) ($P<0.01$), respectively. Neither complete tumor growth regression nor toxicity-induced death was observed in any of the animal groups. However, tumor growth in nude mice treated by the $PHSM^{pop\text{-}upTAT}$ was significantly suppressed, and the size of tumors showed continuous reduction for 12 days. These results are

consistent with the *in vitro* cell viability tests (Fig. 4A), and demonstrate the high cytotoxicity of the $PHSM^{pop\text{-}upTAT}$ at tumor extracellular pH, while correspondingly low cytotoxicity at blood pH. All of the pH-sensitive micelles ($PHSM^{pop\text{-}upTAT}$ and PHSM) showed little influence from differences in on body weight (Supplementary Information, Fig. S-3), indicating low systemic toxicity. Nude mice treated with free DOX exhibited less than 20% loss in body weight after 9 days. Nude mice treated with the $PHSM^{TAT}$ showed about 10% loss over three injections, probably due to non-specific active uptake of the $PHSM^{TAT}$ by normal cells, causing higher systemic toxic effects.

To prove further applicability of the $PHSM^{pop\text{-}upTAT}$, two additional tumor xenograft types (specifically the MCF-7 and human lung tumor A549 cells) were tested in small animals. As shown in Fig. 4B and 4C, the $PHSM^{pop\text{-}upTAT}$ significantly decreased the volume ($P<0.01$, $PHSM^{TAT}$ compared to free DOX) of other two tumors, indicating tumor targeting by the $PHSM^{pop\text{-}upTAT}$ in these tumor types as well. When a similar system coupled with folate ($PHSM^{folate}$) (~ 96 nm size in diameter), was tested with A549 tumors which do not express folate-receptor [33], it was inactive (Fig. 4C) despite having previously proven to be effective for resistant and folate-receptor overexpressing NCI/ADR-RES xenografts [25]. Taken together, these results suggest that the $PHSM^{pop\text{-}upTAT}$ is close to universal in targeting to various acidic solid tumors, independent of the specific antigen presentation or receptor expression profiles.

3.4. In vivo tumor imaging

A dorsal skin-fold window chamber model allows direct *in situ* monitoring of administered drug formulations and visualization of the effects of the various micelles *in vivo* on vascularized tumors [34]. Fluorescein-labeled lipid DHPE was encapsulated within the polymeric micelles to allow for precise fluorescent imaging of the micelles within tumor sites *in vivo*. Fig. 5A supports the tumor-specific accumulation of the $PHSM^{pop\text{-}upTAT}$. Polymeric micelles extravasated from systemic circulation seemed to immediately respond to the acidic interstitial fluid around the tumors, leading to rapid TAT peptide exposure and extensive cellular uptake of the $PHSM^{pop\text{-}upTAT}$. Bright intensity (due to fluorescein DHPE) in the tumor was significant after 60 min, suggesting rapid entry of the $PHSM^{popupTAT}$ into the tumor cells. In contrast, the $PHSM^{TAT}$ showed a relatively lower intensity within the tumors, probably due to less accumulation. Additionally, heterogeneous localization of the $PHSM^{TAT}$ (bright part) was observed, perhaps related to unknown interactions between the cationic TAT peptides and negatively charged biological components around blood vessels [35].

The tumor targeting ability of the $PHSM^{pop\text{-}upTAT}$ was also demonstrated using a near-infrared (NIR) fluorescence imaging system [30]. The NIR fluorescence signals were monitored at scheduled time points after intravenous injection of polymeric micelles in human epidermoid KB tumor-bearing female nude mice (Fig. 5B). The NIR whole-body fluorescence intensity profiles for both the $PHSM^{pop\text{-}upTAT}$ and $PHSM^{TAT}$ were roughly comparable, gradually decreasing during the 24 hours post-injection. However, the tumor-accumulation efficiencies of the $PHSM^{pop\text{-}upTAT}$ and $PHSM^{TAT}$ are different as shown in Fig. 5B. Importantly, the $PHSM^{pop\text{-}upTAT}$ within the KB tumors produces a stronger fluorescence signal and provides more clear images of the tumors, compared to the $PHSM^{TAT}$. This suggests that the tumor targeting efficiency of the $PHSM^{pop\text{-}upTAT}$ is superior to that of the $PHSM^{TAT}$, consistent with the results of *in vivo* tumor suppression

4. Conclusion

Collective results from a series of both *in vitro* and *in vivo* studies strongly support improved, effective treatment of acidic solid tumors, whether they are drug-sensitive or drug-resistant, using the more general targeting nanotechnology enabled by the $PHSM^{pop\text{-}upTAT}$ design.

However, this hypothesis requires further investigation for verification such as *in vivo* manipulation of tumor pH in xenograft and *in vivo* histopathological analysis.

Supplementary Material

Refer to Web version on PubMed Central for supplementary material.

Acknowledgements

The authors thank Profs. D. W. Grainger, C. Lim (Dept of Pharmaceutics, University of Utah), and T. E. Cheatham (Dept of Bioengineering, University of Utah) for their kind discussion/suggestion and proof-reading. This work was supported by NIH CA 122356 and 101850.

References

1. Scholler N, Fu N, Yang Y, Ye Z, Goodman GE, Hellstrom KE, Hellstom I. Soluble member(s) of the mesothelin/megakaryocyte potentiating factor family are detectable in sera from patients with ovarian carcinoma. Proc. Natl. Acad. Sci. USA 1999;96:11531–11536. [PubMed: 10500211]
2. Chaidarun SS, Eggo MC, Sheppard MC, Stewart PM. Expression of epidermal growth factor (EGF), its receptor, and related oncoprotein (erbB-2) in human pituitary tumors and response to EGF in vitro. Endocrinology 1994;135:2012–2021. [PubMed: 7956924]
3. Duncan R. Polymer conjugates as anticancer nanomedicines. Nat. Rev. Cancer 2006;6:688–701. [PubMed: 16900224]
4. Muss HB, Thor AD, Berry DA, Kute T, Liu ET, Koerner F, Cirrincione CT, Budman DR, Wood WC, Barcos M, Henderson IC. c-erbB-2 expression and response to adjuvant therapy in women with node-positive early breast cancer. N. Engl. J. Med 1994;330:1260–1266. [PubMed: 7908410]
5. Daniels RA, Turley H, Kimberley FC, Liu XS, Mongkolsapaya J, Ch'En P, Xu XN, Jin BQ, Pezzella F, Screaton GR. Expression of TRAIL and TRAIL receptors in normal and malignant tissues. Cell Res 2005;15:430–438. [PubMed: 15987601]
6. Parker N, Turk MJ, Westrick E, Lewis JD, Low PS, Leamon CP. Folate receptor expression in carcinomas and normal tissues determined by a quantitative radioligand binding assay. Anal. Biochem 2005;338:284–293. [PubMed: 15745749]
7. Chaudhry A, Carrasquillo JA, Avis IL, Shuke N, Reynolds JC, Bartholomew R, Larson SM, Cuttitta F, Johnson BE, Mulshine JL. Phase I and imaging trial of a monoclonal antibody directed against gastrin-releasing peptide in patients with lung cancer. Clin. Cancer Res 1999;5:3385–3393. [PubMed: 10589749]
8. Fawell S, Seery J, Dajkh Y, Moore C, Chen LL, Pepinsky B, Barsoum B. Tat-mediated delivery of heterologous proteins into cells. Proc. Natl. Acad. Sci. USA 1994;91:664–668. [PubMed: 8290579]
9. Rudolph C, Plank C, Lausier J, Schillinger U, Muller RH, Rosenecker J. Oligomers of the arginine-rich motif of the HIV-1 TAT protein are capable of transferring plasmid DNA into cells. J. Biol. Chem 2003;278:11411–11418. [PubMed: 12519756]
10. Lewin M, Carlesso N, Tun CH, Tang XW, Cory D, Scadden DT, Weissleder R. Tat peptide-derivatized magnetic nanoparticles allow in vivo tracking and recovery of progenitor cells. Nat. Biotechnol 2000;18:410–414. [PubMed: 10748521]
11. Vives E, Richard JP, Rispal C, Lebleu B. TAT peptide internalization: seeking the mechanism of entry. Curr. Protein Pept. Sci 2003;4:125–132. [PubMed: 12678851]
12. Kaplan IM, Wadia JS, Dowdy SF. Cationic TAT peptide transduction domain enters cells by macropinocytosis. J. Control. Release 2005;102:247–253. [PubMed: 15653149]
13. Lee ES, Na K, Bae YH. Super pH-sensitive multifunctional polymeric micelle. Nano Lett 2005;5:325–329. [PubMed: 15794620]
14. Mohajer G, Lee ES, Bae YH. Enhanced intercellular retention activity of novel pH-sensitive polymeric micelles in wild and multidrug resistant MCF-7 cells. Pharm. Res 2007;24:1618–1627. [PubMed: 17385015]

15. Yin H, Lee ES, Kim D, Lee KH, Oh KT, Bae YH. Physicochemical characteristics of pH-sensitive poly(l-Histidine)-b-poly(ethylene glycol)/poly(l-Lactide)-b-poly(ethylene glycol) mixed micelles. J. Control. Release 2008;126:130–138. [PubMed: 18187224]
16. Yang SR, Lee HJ, Kim JD. Histidine-conjugated poly(amino acid) derivatives for the novel endosomolytic delivery carrier of doxorubicin. J. Control. Release 2006;114:60–68. [PubMed: 16828916]
17. van Sluis R, Bhujwalla ZM, Raghunand N, Ballesteros P, Alvarez J, Cerdan S, Galons JP, Gillies RJ. in vivo imaging of extracellular pH using 1H MRSI. Magn. Reson. Med 1999;41:743–750. [PubMed: 10332850]
18. Engin K, Leeper DB, Cater JR, Thistlethwaite AJ, Tupchong L, McFarlane JD. Extracellular pH distribution in human tumours. Int. J. Hyperthermia 1995;11:211–216. [PubMed: 7790735]
19. Leeper DB, Engin K, Thistlethwaite AJ, Hitchon HD, Dover JD, Li D, Tupchong L. Human tumor extracellular pH as a function of blood glucose concentration. Int. J. Radiat. Oncol. Biol. Phys 1994;28:935–943. [PubMed: 8138447]
20. Lee ES, Shin HJ, Na K, Bae YH. Poly(L-histidine)-PEG block copolymer micelles and pH-induced destabilization. J. Control. Release 2003;90:363–374. [PubMed: 12880703]
21. Kim GM, Bae YH, Jo WH. pH-induced Micelle Formation of Poly(histidine-co-phenylalanine)-block-Poly(ethylene glycol) in Aqueous Media. J. Macromol. Biosci 2005;5:1118–1124.
22. Tam JP, Wu CR, Liu W, Zhang JW. Disulfide bond formation in peptides by dimethyl sulfoxide. Scope and application. J. Am. Chem. Soc 1991;113:6657–6662.
23. Sethuraman V, Bae YH. TAT peptide-based micelle system for potential active targeting of anti-cancer agents to acidic solid tumors. J. Control. Release 2007;118:216–224. [PubMed: 17239466]
24. Lee ES, Oh KT, Kim D, Youn YS, Bae YH. Tumor pH-Responsive Flower-Like Micelles of Poly (L-lactic acid)-b-Poly(ethylene glycol)-b-Poly(L-hisitidine). J. Control. Release 2007;123:19–26. [PubMed: 17826863]
25. Lee ES, Na K, Bae YH. Doxorubicin loaded smart polymeric micelles for reversal of resistant MCF-7 tumor. J. Control. Release 2005;103:405–418. [PubMed: 15763623]
26. Szakacs G, Paterson JK, Ludwig JA, Booth-Genthe C, Gottesman MM. Targeting multidrug resistance in cancer. Nat. Rev. Drug Discov 2006;5:219–234. [PubMed: 16518375]
27. Desoize B, Jardillier JC. Multicellular resistance: a paradigm for clinical resistance? Crit. Rev. Oncol. Hemat 2000;36:193–207.
28. Dreher MR, Liu W, Michelich CR, Dewhirst MW, Yuan F, Chilkoti A. Tumor vascular permeability, accumulation, and penetration of macromolecular drug carriers. J. Natl. Cancer Inst 2006;98:335–344. [PubMed: 16507830]
29. Shan S, Sorg B, Dewhirst MW. A novel rodent mammary window of orthotopic breast cancer for intravital microscopy. Microvasc. Res 2003;65:109–117. [PubMed: 12686168]
30. Park K, Kim JH, Nam YS, Lee S, Nam HY, Kim K, Park JH, Kim IS, Choi K, Kim SY, Kwon IC. Effect of polymer molecular weight on the tumor targeting characteristics of self-assembled glycol chitosan nanoparticles. J. Control. Release 2007;122:305–314. [PubMed: 17643545]
31. Mehta K, Devarajan E, Chen J, Multani A, Pathak S. Multidrug-resistant MCF-7 cells: an identity crisis. J. Natl. Cancer Inst 2002;94:1652–1654. [PubMed: 12419794]
32. Mahadevan D, List AF. Targeting the multidrug resistance-1 transporter in AML: molecular regulation and therapeutic strategies. Blood 2004;104:1940–1951. [PubMed: 15217827]
33. Oh IK, Mok H, Park TG. Folate immobilized and PEGylated adenovirus for retargeting to tumor cells. Bioconjug. Chem 2006;17:721–727. [PubMed: 16704210]
34. Dreher MR, Liu W, Michelich CR, Dewhirst MW, Chilkoti A. Thermal cycling enhances the accumulation of a temperature-sensitive biopolymer in solid tumors. Cancer Res 2007;67:4418–4424. [PubMed: 17483356]
35. Ziegler A, Seelig J. Interaction of protein transduction domain of HIV-1 TAT with heparan sulfate. Binding mechanism and thermodynamic parameters. Biophys. J 2004;86:254–263. [PubMed: 14695267]

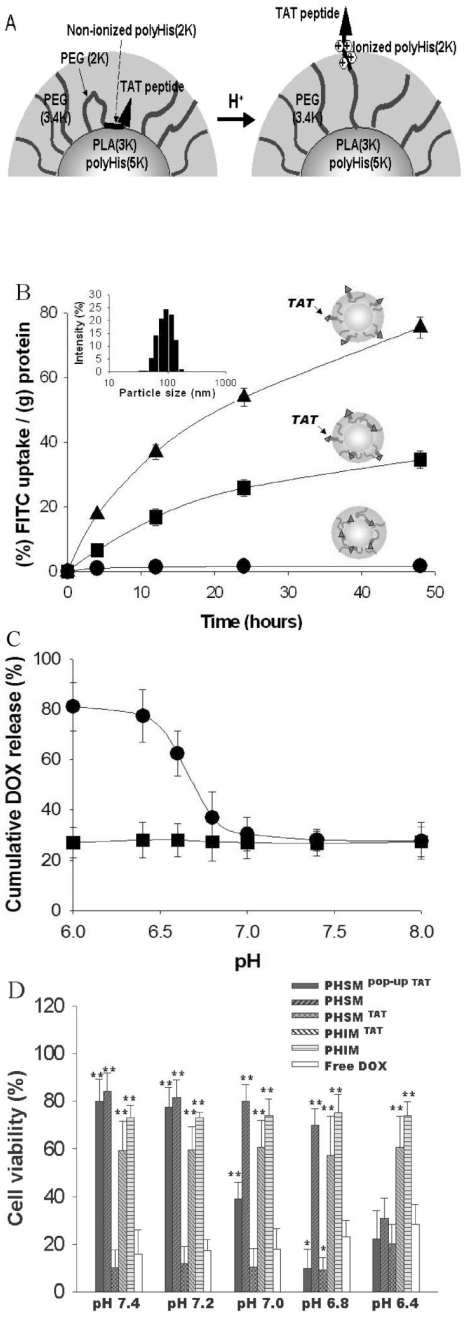

Fig. 1.

pH-sensitivity for polymeric micelle drug targeting of drug-sensitive tumor. **(A)** Schematic representation of the acid-induced pop-up targeting mechanism for the peptide-conjugated micelle corona. **(B)** Cellular uptake of PHSM$^{pop\text{-}upTAT}$ in cultured MCF-7 cells: pH 7.4 **(●)**, pH 7.0 **(■)**, pH 6.8 **(▲)**. Particle size and size distributions of PHSM$^{pop\text{-}upTAT}$ suspensions (in PBS) at pH 7.4 were measured by dynamic light scattering. Each data point represents an average with standard deviation (n=3). (**C**) Cumulative DOX release from PHSM$^{pop\text{-}upTAT}$ (●) with decreasing pH. PHIM^{TAT} (■) was used as a control group (n=3). (**D**) Drug-sensitive MCF-7 cell killing efficacy of PHSM$^{pop\text{-}upTAT}$ (DOX 10 μg/ml equivalent) as a function of

pH after 48-hour incubation. Five control experiments (PHSM, $PHSM^{TAT}$, $PHIM^{TAT}$, PHIM, and free DOX) were conducted (n=9) (*$p < 0.05$, **$p < 0.01$ compared to free DOX).

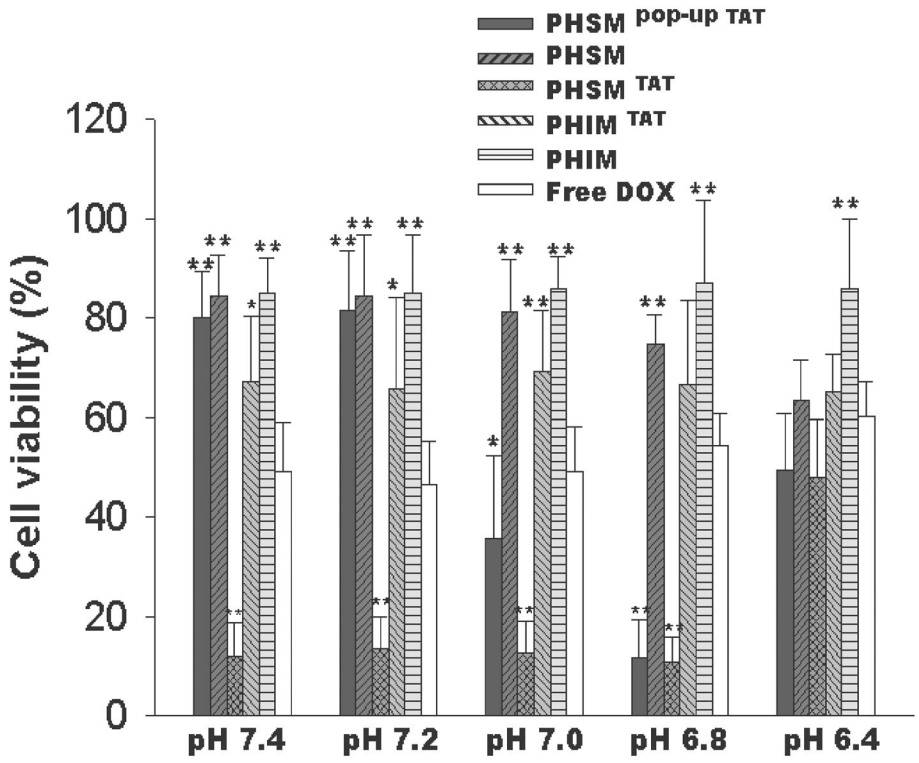

Fig. 2.

pH-sensitivity for polymeric micelle drug targeting of drug-resistant tumor. Drug-resistant NCI/ADR-RES cell killing efficacy of $PHSM^{pop\text{-}up TAT}$ (DOX 10 μg/ml equivalent) as a function of pH after 48-hour incubation. Five control experiments (PHSM, $PHSM^{TAT}$, $PHIM^{TAT}$, PHIM, and free DOX) were conducted. Each data point represents an average with standard deviation (n=9) (*$p < 0.05$, **$p < 0.01$ compared to free DOX).

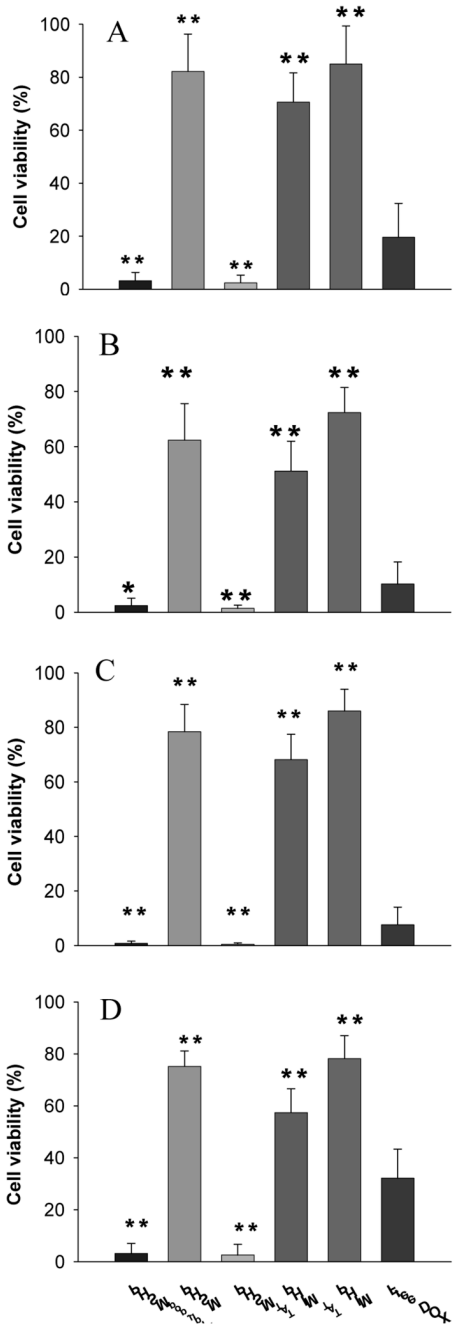

Fig. 3.

Reversing various MDR mechanisms using polymer micelles in cell culture. **(A)** Cytotoxicity of $PHSM^{pop\text{-}upTAT}$ with a DOX 5 μg/ml equivalent against HL-60/MX2 cells (altered Topo II expression) after 1-hour incubation, **(B)** with a DOX 1 μg/ml equivalent against HL-60 cells (bcl-2 positive expression) after 1-hour incubation, **(C)** with a DOX 5 μg/ml equivalent against NCI-H69/AR cells (MRP expression) after 24-hour incubation and **(D)** with a DOX 10 μg/ml equivalent against A549 cells (LRP expression) after 48-hour incubation. All experiments were performed at pH 6.8 RPMI-1640/PBS medium. Five control experiments (PHSM, $PHSM^{TAT}$, $PHIM^{TAT}$, PHIM, and free DOX) were also conducted (n=9) (*$p < 0.05$, **$p < 0.01$ compared to free DOX).

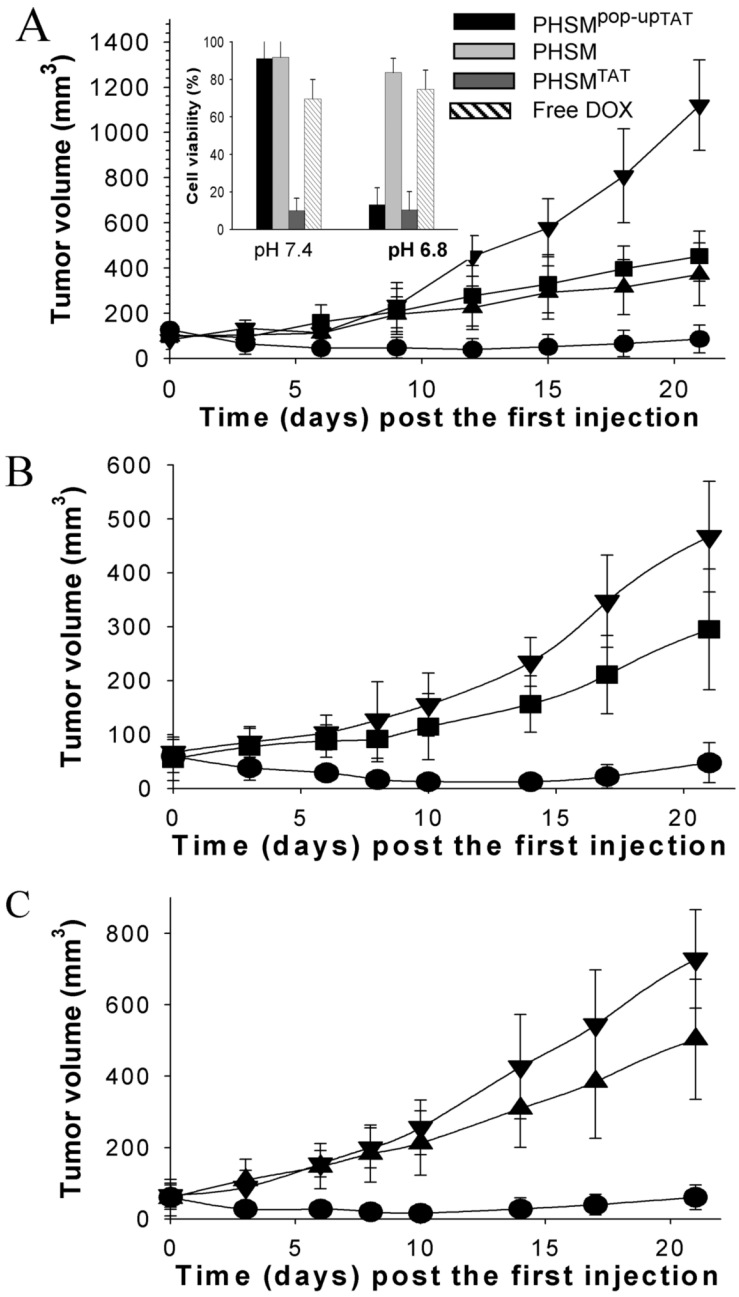

Fig. 4.

In vivo efficacy against solid tumors. **(A)** Tumor regression by $PHSM^{pop\text{-}upTAT}$. $PHSM^{pop\text{-}upTAT}$ **(●)** (equivalent DOX 10 mg/kg body) was intravenously injected three times (days 0, 3 and 6 post the first injection) to nude mice bearing A2780/AD tumor xenografts (n=4). Three controls experiments (PHSM (■), $PHSM^{TAT}$ **(▲)** and free DOX **(▼)**) were also conducted. *In vitro* cytotoxicities of $PHSM^{pop\text{-}upTAT}$, PHSM, $PHSM^{TAT}$ and free DOX are shown (inset figure). Samples with DOX 1 μg/ml equivalent were applied to A2780/AD cells for 48 hours (*$p < 0.05$, **$p < 0.01$ compared to free DOX) (n=9). Similar tumor regression tests (under the same conditions) using $PHSM^{pop\text{-}upTAT}$ **(●)** were performed for nude mice

bearing (**B**) MCF-7 tumor (n=4) and (**C**) A549 tumor xenografts (n=4). Control experiments ($PHSM^{TAT}$ **(■)**, $PHSM^{folate}$ **(▲)** and free DOX **(▼)**) were co-conducted in (B) and (C).

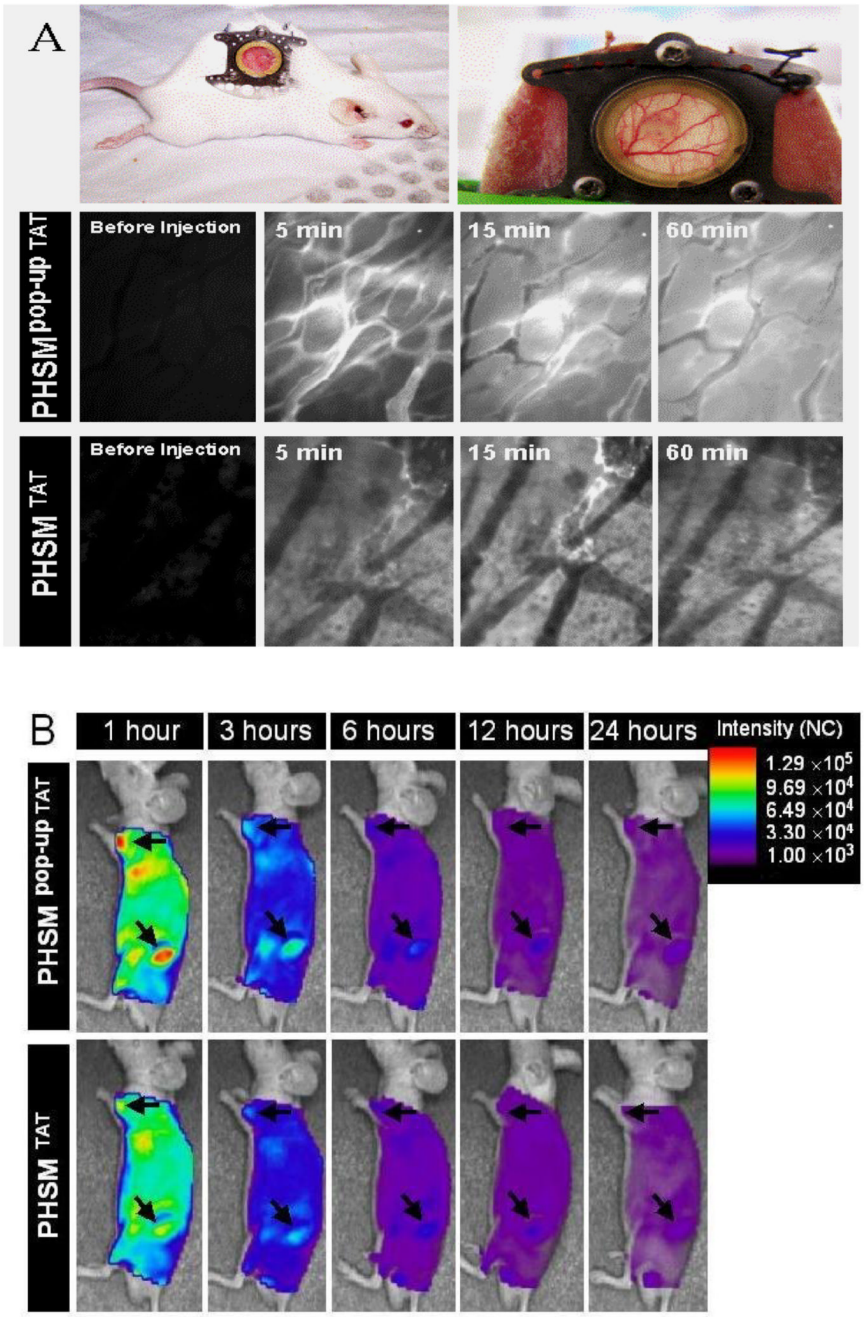

Fig. 5.

In vivo imaging solid tumors. **(A)** *In vivo* dorsal window chamber imaging of nude mice bearing MCF-7 cell xenograft tumors over time (5, 15, 60 min); $PHSM^{pop\text{-}upTAT}$ and $PHSM^{TAT}$ micelles' tumor penetration imaged *in situ* by FITC fluorescence. **(B)** *In vivo* NIR fluorescence real-time imaging of nude mice bearing KB tumor xenografts. Two tumor sites are indicated by arrows. Intensity levels of micelle with Cy5.5® are depicted in the figure.

Table 1

IC_{50} of $PHSM^{pop\text{-}upTAT}$ and free DOX for HL-60/MX2, HL-60, NCI-H69/AR, and A549 MDR cells (n=9). All experiments were performed at pH 6.8 RPMI-1640/PBS medium. IC_{50} was obtained from the DOX concentration where 50% cell viability was achieved [24,26].

	$PHSM^{pop\text{-}upTAT}$	Free DOX
HL-60/MX2[a]	0.32±0.07 μg/ml	1.12±0.08 μg/ml
HL-60[b]	0.10±0.03 μg/ml	0.42±0.07 μg/ml
NCI-H69/AR[c]	0.20±0.06 μg/ml	0.75±0.08 μg/ml
A549[d]	0.75±0.08 μg/ml	6.60±0.09 μg/ml

[a] after 1-hour incubation

[b] after 1-hour incubation

[c] after 24-hour incubation

[d] after 48-hour incubation.